Ultimate Intrinsic Signal-to-Noise Ratio in MRI

Ogan Ocali, Ergin Atalar

A method to calculate the ultimate intrinsic signal-to-noise ratio (SNR) in a magnetic resonance experiment for a point inside an arbitrarily shaped object is presented. The ultimate intrinsic SNR is determined by body noise. A solution is obtained by optimizing the electromagnetic field to minimize total power deposition while maintaining a constant right-hand circularly polarized component of the magnetic field at the point of interest. A numerical approximation for the optimal field is found by assuming a superposition of a large number of plane waves. This simulation allowed estimation of the ultimate intrinsic SNR attainable in a human torso model. The performance of six coil configurations was evaluated by comparing the SNR of images obtained by the coils with the ultimate values. In addition, the behavior of ultimate intrinsic SNR was investigated as a function of main field strength. It was found that the ultimate intrinsic SNR increases better than linearly with the main magnetic field up to 10 T for our model. It was observed that for field strengths of 4 T or higher, focusing is required to reach the ultimate intrinsic SNR.

Key words: SNR optimization; RF coil design; skin effect; focusing

INTRODUCTION

A fidelity measure that is independent of imaging parameters and the signal processing system is needed to compare and evaluate magnetic resonance (MR) sensors accurately. Such a measure is the intrinsic signal-to-noise ratio (SNR), defined for a given sample-antenna combination as the MR signal voltage received from a 1-cm cube of sample divided by the root-mean-square (RMS) noise voltage received per square-root hertz of bandwidth (1). In modern MRI systems, intrinsic SNR is the limiting factor in image quality. Intrinsic SNR depends on the coil geometry even if the coil noise is excluded. The *ultimate* possible value of intrinsic SNR for a sample with given shape and electrical properties, however, is independent of coil design. By comparing the ultimate intrinsic SNR value with the intrinsic SNR of a coil under development, the coil designer can decide whether there is room for further improvement.

In addition, knowledge of the ultimate intrinsic SNR value can be used to determine the achievable SNR values as a function of the field strength. At each field strength a different coil configuration may be optimum. It is reasonable to assume that coils that perform close to the optimum will be used for each field strength. Hence, in comparing different main field strength systems the ultimate intrinsic SNR is a helpful measure.

For a fixed receiver coil configuration, quasistatic analysis predicts that the intrinsic SNR is linearly dependent on the main magnetic field strength, since, under quasistatic conditions, both MR signal and power loss increase with the square of field strength (1, 2). Quasistatic analysis yields accurate results only for low field strength in which the wavelength is much larger than the body size. At high field strengths, the MR signal has to traverse lossy media before reaching the MR antenna, which causes a signal drop, called the *skin effect*. In addition, the phase of the signal from different parts of the sample will deviate (3, 4). Contrary to what might be assumed, the skin effect may give rise to an increase in SNR if the point of interest is close to the surface of the sample by effectively screening the noise that is generated inside the sample (5). When the point of interest is in the center of the sample, however, it might seem that intrinsic SNR would be less than linearly dependent on magnetic field strength. In this paper, we show that this assumption is incorrect.

The noise level is determined by dissipative power losses in the system. There are various dissipation mechanisms that cause power loss, including conductor losses, body losses, and radiation losses. Each loss mechanism contributes to the resistance in the equivalent circuit. For properly designed systems, the limiting loss mechanism (most significant noise source), should be the body losses. Other losses can be reduced to insignificant levels by use of proper materials, carefully designed coil geometry, and low-noise electronic components. The ultimate value of the intrinsic SNR depends only on body losses.

For a given body shape, a straightforward approach to SNR optimization is to design the receiver antenna with a number of unknown parameters (height, radius, etc.), calculate the SNR parametrically, and determine the optimal values for those parameters. However, in the process, one has to solve the associated electromagnetic field equations in terms of unknown parameters, which is a formidable task even for the simplest of shapes and even with simplified approximations. Hence, the common approach is to assume quasistatic conditions and body shape to be a semi-infinite plane (2, 6, 7), or an infinite length cylinder. However, as we will show, these assumptions lose validity even at moderate field strengths ($\geq$0.5 T). Moreover, this approach gives optimal SNR for only the chosen antenna configuration, which must be determined carefully before the parametric optimization.

We solve the problem for an arbitrary body shape with uniform electrical properties. Although the second assumption is unrealistic, if the wavelength is larger than the internal structural heterogeneity dimensions or the

MRM 39:462–473 (1998)

From the Johns Hopkins University School of Medicine, Department of Radiology, Baltimore, Maryland.

Address correspondence to: Ergin Atalar, Ph.D., Department of Radiology, Johns Hopkins University School of Medicine, 601 N. Caroline Street, JHOC 4241, Baltimore, MD 21287-0845.

Received October 15, 1997; revised September 4, 1997; accepted September 8, 1997.

This work was supported by the Whitaker Foundation.

0740-3194/98 $3.00

differences in electrical properties are not too great, this assumption is valid.

The intrinsic signal and noise voltages can be determined with only the knowledge of the electromagnetic fields generated by the receiver antenna when it is used as a transmitter antenna using the reciprocity principle (5). When body noise is predominant, SNR optimization is equivalent to the constrained optimization problem of minimizing total power deposited in the body, under the constraint of having a fixed value for the transverse, circularly polarized component of the magnetic field at the point of interest. Therefore, instead of parametrically optimizing the receiver antenna, we perform the optimization over the electromagnetic field, regardless of the receiver antenna structure. Surprisingly, the problem of determining the optimal electromagnetic field is a much easier task than determining the electromagnetic field generated by a given MR coil. The solution to the above optimization problem gives us the electromagnetic field generated by the optimal MR coil when used as a transmitter antenna. The optimal electromagnetic field depends on the location of the point of interest as well as the shape and electromagnetic properties of the body.

We assume that the optimal electromagnetic field can be expressed as a linear combination of a finite number of plane waves, which serve as basis functions. The optimization problem then becomes that of determining the optimal weight of each plane wave. In terms of mathematical operations, this method is equivalent to determining the optimal weights of a linear array of coils of which each coil generates one of the plane waves when used as a transmitter with unity current at its terminals.

THEORY

The signal voltage amplitude from a 1-ml voxel of sample in an MRI experiment is given as

$$v_S = \omega\mu|\mathbf{H}\cdot\mathbf{M}| \qquad [1]$$

using the reciprocity principle (5). v_S is the signal voltage, $\mathbf{M}$ is the total transverse nuclear magnetic moment vector in 1 ml of sample, μ is the magnetic permeability of the sample, ω is the operating Larmor frequency of the nuclei of interest, and $\mathbf{H}$ is the magnetic field generated by the coil at unit input current. In Eq. [1], $\mathbf{H}$ and $\mathbf{M}$ are complex valued, phasor domain vectors, and their inner product is considered.

Assuming the main magnetic field is in the z direction, we can write the magnetic moment of the sample voxel as

$$\mathbf{M} = M_0\hat{\mathbf{u}}_x - jM_0\hat{\mathbf{u}}_y$$

which corresponds to a time domain rotating magnetic moment of

$$\overline{\mathbf{M}}(t) = M_0\cos(\omega t + \phi)\hat{\mathbf{u}}_x - M_0\sin(\omega t + \phi)\hat{\mathbf{u}}_y$$

ϕ being an arbitrary reference phase. M_0 is the instantaneous magnitude of the time domain magnetic moment in the sample voxel, immediately after the application of an ideal 90° pulse. The signal drop due to finite values of T_1 and T_2 are not included in $\mathbf{M}$.

H can be decomposed into its right- and left-hand circularly polarized components

$$\mathbf{H} = H_+\hat{\mathbf{u}}_+ + H_-\hat{\mathbf{u}}_-$$

where the unit right- and left-hand polarized vectors are given as $\hat{\mathbf{u}}_\pm = (\hat{\mathbf{u}}_x \pm j\hat{\mathbf{u}}_y)/\sqrt{2}$ and the right- and left-hand polarized components of H $H_\pm = (H_x \pm H_y)/\sqrt{2}$. The signal voltage in Eq. [1] can be expressed in terms of M_0 and the right-hand circularly polarized component of the magnetic field as

$$v_s = \sqrt{2}\omega\mu M_0 H_+ \qquad [2]$$

The RMS noise voltage per one square-root Hertz can be calculated as

$$v_N = \sqrt{4k_B TR}, \qquad [3]$$

where k_B is the Boltzmann constant, T is the sample temperature, and R is the real part of the input impedance seen from the input terminals of the coil. The intrinsic SNR becomes (1)

$$\Psi = \frac{v_S}{v_N} \propto \frac{H_+}{\sqrt{R}} \qquad [4]$$

The only coil-dependent parameters that affect the SNR are R and H_+. To improve SNR we must increase H and decrease R, which are usually conflicting goals in receiver coil design.

Note that the observed SNR in the resulting images is given as

$$SNR = \Psi\frac{V\sqrt{N_x N_y\, NEX}}{F\sqrt{2BW}}, \qquad [5]$$

where $F > 1$ is the system noise figure, V is the sample volume in milliliters, where NEX is the number of image repetitions, N_x, N_y are the number of readout points and phase encoding steps, respectively, and $\pm BW$ is the receiver bandwidth. Observe that this expression accounts for the noise reduction due to effective data averaging that is performed during image reconstruction. In practice, where magnitude images are displayed, SNR on the images approach the value given by Eq. [4] only at the bright locations where SNR is large (8).

The value of R in Eq. [3] can be found by evaluating the total dissipated power when the MR receiver is used as a transmitter antenna with unit current at its terminals,

$$R = P_{\text{loss}} \qquad [6]$$

In mechanisms causing power loss, only body noise determines the ultimate value of the intrinsic SNR.

Assuming that the body does not contain any lossy magnetic material, which is a good approximation for living tissue, the power deposited in the body can be evaluated as

$$R_{\text{body}} = \int_{\text{body}} |\mathbf{E}(\mathbf{r})|^2\,\sigma\,dv \qquad [7]$$

where **E(r)** denotes the electric field at point **r**, σ is the conductivity, and the integral is evaluated over the body volume.

To find the ultimate possible value of intrinsic SNR, we minimize the value of R_{body} while having a fixed value of signal voltage, v_s, in Eq. [4]. The optimization is performed over the electromagnetic field set up by the antenna when it is used to transmit with unit current at its input.

We assume that the main magnetization is parallel to the z axis. The optimization is performed over electromagnetic fields **E(r)** and **H(r)** that satisfy the phasor domain Maxwell's Eq. [9] inside a given body shape:

$$\nabla \times \mathbf{H}(\mathbf{r}) = (\sigma + j\omega\epsilon)\mathbf{E}(\mathbf{r}) \quad [8]$$

$$\nabla \times \mathbf{E}(\mathbf{r}) = -j\omega\mu_0\mathbf{H}(\mathbf{r}) \quad [9]$$

The optimal electromagnetic field can be scaled arbitrarily without changing its optimality, allowing us to normalize the right-hand circularly polarized component of the magnetic field at the point of interest, $\boldsymbol{r}_0$, to unity, e.g., $H_+(r_0) = 1$.

It can be shown (Appendix A) that the problem of determining the ultimate SNR is reduced to finding **H(r), E(r)** such that for *all* test fields, $\mathbf{H}_T$, $\mathbf{E}_T$, that also satisfy the Maxwell's equations, the following equation holds:

$$\int_{\text{body}} \mathbf{E}^*(\mathbf{r})\mathbf{E}_T(\mathbf{r})\sigma \mathrm{d}v = \lambda(H_{T+}(\mathbf{r}_0)) \quad [10]$$

where

$$\lambda = \int_{\text{body}} |\mathbf{E}(\mathbf{r})|^2\sigma \, \mathrm{d}v \quad [11]$$

and H_{T+} denotes the right-hand circularly polarized component of the test magnetic field. Observe that λ is independent of the test field, $\mathbf{H}_T$, $\mathbf{E}_T$, and the optimality condition provides a relationship between all test fields and the optimal field, **H(r), E(r).**

If the optimality condition is satisfied, SNR cannot be improved by the addition of any coil, nor by any means of signal combination.

The aim of this method is to determine the electromagnetic field that satisfies this optimality condition. To that end we approximate the solution as a superposition of modes (basis functions) with unknown coefficients (weights) as in the mode matching method (MMM), which is used in analysis of electromagnetic wave problems (10). In the MMM, the weights are determined by using the boundary conditions, whereas in our method the weights are determined by using the optimality condition. The reliability of the modal expansion depends on the type of problem and the chosen basis functions. A rigorous analysis of reliability and practicability of various mode sets for various problems is given in ref. 10.

For our problem, in the interior of a given source-free finite volume, assuming a homogeneous medium, it is possible to express the electromagnetic field solution as an infinite linear combination of plane waves (10–12):

$$\mathbf{E}(\mathbf{r}) = \sum_i^{\infty} \alpha_i\mathbf{E}_i(\mathbf{r}) \quad [12]$$

$$\mathbf{H}(\mathbf{r}) = \sum_i^{\infty} \alpha_i\mathbf{H}_i(\mathbf{r}) \quad [13]$$

where $\mathbf{E}_i(\mathbf{r})$ and $\mathbf{H}_i(\mathbf{r})$ represent RMS electric and magnetic fields associated with the i^{th} mode, which we assume to be a plane wave propagating in the $\mathbf{k}_i$ direction

$$\mathbf{E}_i(\mathbf{r}) = \mathbf{E}_{i0}e^{-j[\mathbf{k}_i\cdot\mathbf{r}]}e^{j\omega t} \quad [14]$$

$$\mathbf{H}_i(\mathbf{r}) = \mathbf{H}_{i0}e^{-j[\mathbf{k}_i\cdot\mathbf{r}]}e^{j\omega t} \quad [15]$$

where $\mathbf{E}_{i0}$, $\mathbf{H}_{i0}$ are constant vectors and are related to k_i by Maxwell's equations, and α_i are gains associated with each plane wave. Unlike the mode matching method, we use the optimality condition to solve for the unknown weights. For each propagation direction two plane waves of orthogonal polarizations are included in the mode set. Equivalently each propagation direction is repeated in the mode set with different $\mathbf{E}_{i0}$ and $\mathbf{H}_{i0}$.

To make the problem amenable to numerical computation, we assume that the solution can be expressed as a linear combination of a finite number of plane waves, simply by restricting the upper limit of the summations in Eqs. [12] and [13] to a finite number. Note that any required precision can be achieved by increasing the number of modes. Also note that it is possible to choose other sets of vector basis functions for special cases to improve speed and accuracy, e.g., Bessel functions for cylindrical symmetric problems or spherical harmonics for a sphere, etc. (10). In our examples the plane waves are preferred because of their completeness and simplicity. Results of numerical computations suggest that the plane wave expansion is a good approximation when the point of interest is more than 0.01 wavelengths away from the boundaries.

We assume that the body under consideration has a magnetic permeability equal to that of free space; thus, inserting Eqs. [14] and [15] into Maxwell's Eqs. [8] and [9] (each individual mode has to satisfy Maxwell's equations) one obtains

$$\mathbf{H}_{i0} = \frac{1}{j\omega\mu_0}\mathbf{k}_i \times \mathbf{E}_{i0} \quad [16]$$

$$\mathbf{k}_i \cdot \mathbf{k}_i = -j\omega\mu_0[\sigma + j\omega\epsilon] \quad [17]$$

$$\mathbf{E}_{i0} \cdot \mathbf{k}_i = 0 \quad [18]$$

We choose the wave vectors $\mathbf{k}_i$ as

$$\mathbf{k}_i = \bar{\mathbf{k}}_i\sqrt{-j\omega\mu_0[\sigma + j\omega\epsilon]} \quad [19]$$

where $\bar{\mathbf{k}}_i$ is a real unit vector in the three dimensions for each i. The two polarization directions for each wave vector can be chosen arbitrarily, as long as they are orthogonal to each other.

One may interpret each $\mathbf{k}_i$ vector as a directional antenna placed far away from the body pointing toward the body. The direction of plane waves, $\bar{\mathbf{k}}_i$, must be chosen such that the plane waves set achieves good coverage of the search space. We distribute the wave vectors over the surface of a sphere evenly.

Once the directions and the number of plane waves are selected, assuming that σ is independent of position, body noise resistance can be written as

$$R_{\text{body}} = \sigma \int_{\text{body}} \|\mathbf{E}(\mathbf{r})\|^2 dv \quad [20]$$

$$= \sigma \int_{\text{body}} \|\sum_i \alpha_i \mathbf{E}_i(\mathbf{r})\|^2 dv \quad [21]$$

$$= \sum_i \sum_j \alpha_i^* \alpha_j \{ \int_{\text{body}} \mathbf{E}_i(\mathbf{r})^* \mathbf{E}_j(\mathbf{r}) dv \} \quad [22]$$

$$= \alpha^{*T} \mathbf{R} \alpha \quad [23]$$

where $\alpha = [\alpha_1, \alpha_2, \cdots, \alpha_n]^T$ is the coefficient vector, each element is the weight of the corresponding plane wave, and $\mathbf{R}$ is the noise correlation matrix related to the plane waves (13)

$$R_{ij} = \sigma \int_{\text{body}} \mathbf{E}_i(\mathbf{r})^* \mathbf{E}_j(\mathbf{r}) dv \quad [24]$$

Finding the ultimate intrinsic SNR becomes a task of minimizing the total power loss or the equivalent noise resistance

$$R_{\min} = \min \alpha^{*T} \mathbf{R} \alpha \quad [25]$$

subject to

$$H_+(\mathbf{r}_0) = \sum_i \alpha_i H_{i+}(\mathbf{r}_0) = \mathbf{b}\alpha = 1 \quad [26]$$

where the computation of $\mathbf{R}$, $\mathbf{b} = [H_{0+}, H_{1+}, H_{2+}, \ldots, H_{n+}]$ is presented in Appendix B for various shapes. The optimal gain vector, α_{opt}, is then computed as

$$\alpha_{\text{opt}} = \frac{\mathbf{R}^{-1}\mathbf{b}^{*T}}{\mathbf{b}\mathbf{R}^{-1}\mathbf{b}^{*T}} \quad [27]$$

Finally the value of the total dissipated power or the noise resistance, $\mathbf{R}$, is found by

$$R_{\min} = \alpha_{\text{opt}}^T \mathbf{R} \alpha_{\text{opt}} = \frac{1}{\mathbf{b}\mathbf{R}^{-1}\mathbf{b}^{*T}} \quad [28]$$

from which the value of the ultimate intrinsic SNR can be determined as

$$\Psi_{\max} = \frac{\sqrt{2\omega\mu_0 M_0}}{\sqrt{4k_B T R_{\min}}} \quad [29]$$

ALGORITHM

Determination of the maximal SNR and the optimal electromagnetic field is performed as described in the following steps: (1) (Input) Obtain the shape and electrical properties of the object at the operating frequency; (2) Select wave-vectors, $\mathbf{k}_i$, as in Eq. [19] and polarization directions; (3) Set up the matrix $\mathbf{R}$ in the linear equation as shown in Eq. [24] and Appendix B, or follow the lines of Appendix B numerically; (4) Set up the matrix $\mathbf{b}$ as in Eq. [26] using the coordinates of the point of interest, at which SNR will be optimized; (5) Solve the equations to get the optimal coefficient vector, α, as in Eq. [27]. (6) If desired, determine the electromagnetic field as the optimal linear combination of the plane wave modes as in Eqs. [12] and [13]. (7) Find the value of $\Phi_{\max}$ using Eq. [28]. (8) Repeat steps 4–7 for all desired points of interest to get a map of ultimate SNR.

In step 2, as the number of plane waves grows, the resulting set of equations will be more difficult to solve numerically, because each mode will have closer neighbors and the equations will be closer to being linearly dependent. As the number of modes increases, the numerical precision of the computer operations must increase. Conversely, the number of modes chosen should be as high as possible to avoid discretization errors. As the number of modes decreases, the precision of approximating the solution as a linear combination of the chosen modes will decrease. As the number of modes increases, the resulting SNR eventually saturates (when using double precision number representation), usually before the point where the solution to the linear equation set becomes impossible due to numerical errors such as truncation and round-off.

In step 3, the matrix $\mathbf{R}$ is conjugate symmetric, hence only about half of the elements are actually calculated, and the rest of the matrix elements are determined by complex-conjugation. For step 5, we recommend the use of a high precision linear equation solver. This equation set is inherently difficult to solve. The numerical errors can be decreased either by decreasing the number of modes or increasing the precision of the number representation.

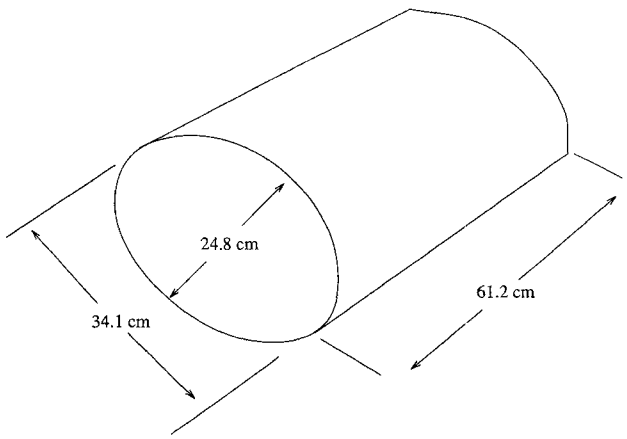

FIG. 1. Human torso model. The cylinder has an elliptic profile and is filled with a NaCl solution.

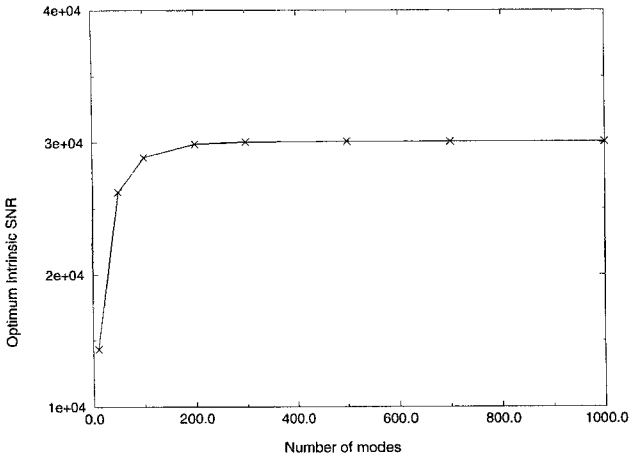

FIG. 2. Optimal value of the intrinsic SNR versus number of modes used in the simulation. Note the saturation after number of modes exceeds 200.

APPLICATIONS

Coil Performance Map

The ultimate intrinsic SNR provides a useful absolute reference value for coil performance evaluation. In general, ultimate intrinsic SNR is a position-dependent number; thus, at each point the relative performance of a given coil to the optimal field is different. We propose the use of a coil performance map (CPM), which is defined as the ratio of the actual obtained SNR to the ultimate intrinsic SNR as a function of space. This map provides position-dependent relative performance information. Using this information, it is possible to make various design decisions, such as element size and placement, or to determine the best place to use the coil.

We performed ultimate intrinsic SNR computations for a human torso model. The model was a *finite* cylinder with an elliptic profile, filled with a material that had conductive loss and dimensions similar to that of an adult human torso, as seen in Fig. 1. We took the effective conductance as $\sigma = 0.37\ (\Omega m)^{-1}$ as representative of average human tissue conductivity and assumed a proton MR susceptibility of 3×10^{-9}, which is very close to that of water (14). We used a relative dielectric constant of 77.7.

We placed the torso axis in the z direction, parallel to the main magnetic field, and the long axis of the ellipse was in the x direction. We took the points of interest axially in the x-y plane at the midsection of the torso. We chose the number of modes in the computations in a

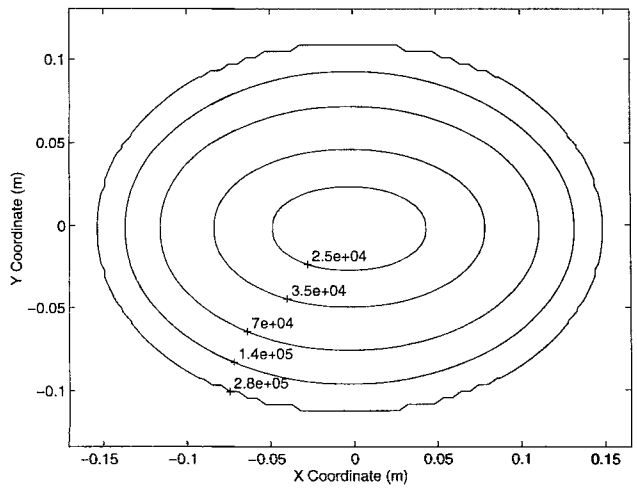

FIG. 3. Ultimate intrinsic SNR as a function of position of the point of interest inside the torso model.

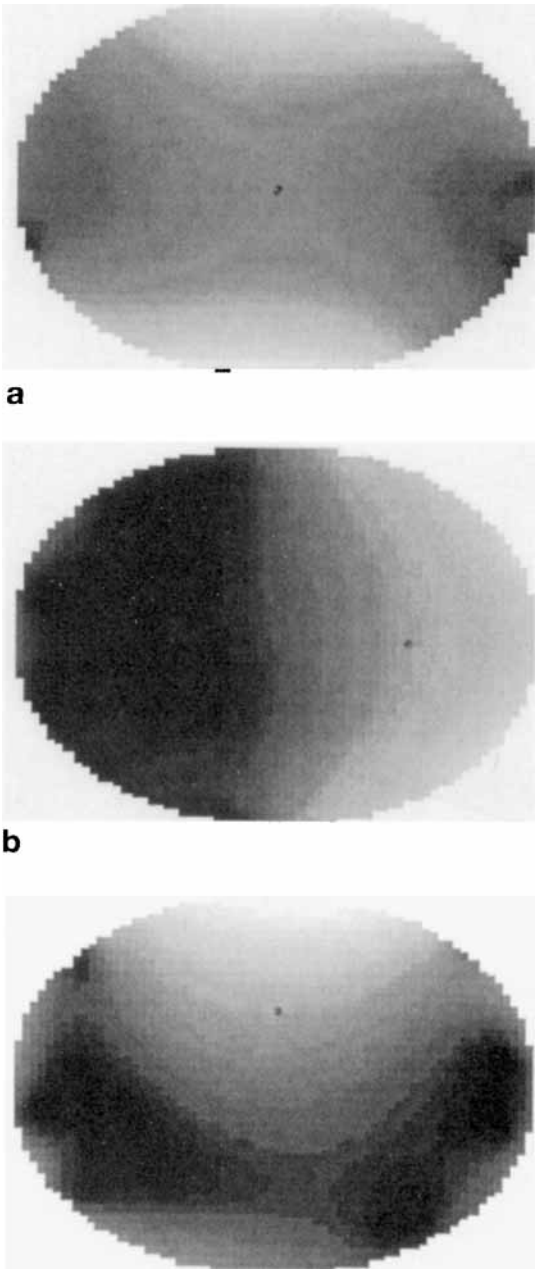

FIG. 4. The right-hand polarized component of the magnetic field (sensitivity) in the solution field for the point of interest (a) at the center, (b) at x = 7, y = 0 cm, (c) at x = 0, y = 5 cm. Note that in the optimal field the sensitivity has a maximum at the edge closest to the point of interest.

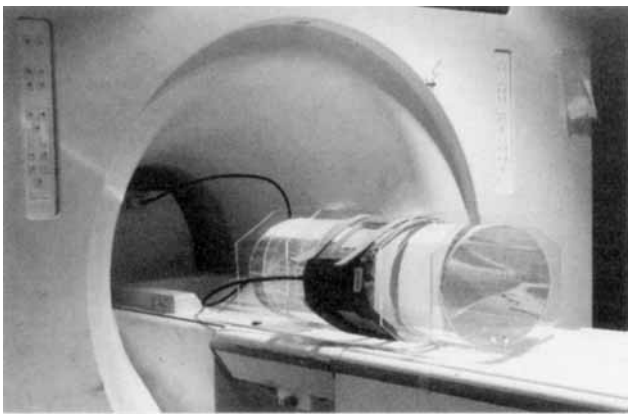

FIG. 5. The human torso phantom with a gpflex coil placed at the midsection. The surrounding rings are for mechanical stability.

range of 200–500, depending on the point of interest. In Fig. 2 the optimal value of the intrinsic SNR, as the result of the simulation at $x = 5$ cm versus number of modes at 1.5 T is shown. From this plot, it is seen that the optimal intrinsic SNR saturates after the number of modes exceeds 200–300. The value of the ultimate intrinsic SNR versus point position at 1.5 T is shown as a contour map in Fig. 3. At the points very close to the surface (≈1 cm), the $\mathbf{R}^{-1}\, b$ calculation gave large numerical errors before reaching the steady-state values of the ultimate intrinsic SNR; thus, the results in that crux are unreliable. Observe that the ultimate intrinsic SNR increases as the point of interest gets closer to the surface of the sample. Also note that for each different point, the simulation results in a different optimal electromagnetic field, meaning that for each point of interest there is a unique coil configuration that optimizes the SNR. In Fig. 4 we depict the right-hand polarized component of the magnetic field in the x, y field, as an intensity map at 1.5 T for three different points of interest. These maps provide an intuitive idea about the coil structure and placement necessary to achieve the ultimate intrinsic SNR.

We next constructed a phantom whose dimensions matched the torso model (see Fig. 5). The phantom was filled with tap water, and 76.6 g of NaCl was added for electrical loading. With this loading, the normality of the salt became 0.0322 Eq/liter. Using modified Stogyrin expressions (15), we obtained a conductance of $\sigma = 0.372$ and a relative dielectric constant of $\epsilon_r = 77.7$, which lie in the human tissue parameter range at 1.5 T. The phantom was constructed of Plexiglas because of its ideal mechanical and electrical properties. The phantom was imaged using various coils, with a pulse sequence that minimized T_1, T_2 effects. We used a fast spin echo sequence with a TR of 6 s and a TE of 14 msec, 256 × 256 data acquisition matrix, and 1 NEX. The images of the torso phantom using the body coil, a 5-inch dual coil with two different coil placements, a commercial flexible coil from GE (gpflex), and an optimized experimental cardiac phased array (16) at 1.5 T using a GE Signa Horizon system are shown in Figs. 6–10.

To measure the noise level, a difference image is obtained by subtracting the original image from another image of the same slice taken with the same imaging parameters immediately after the first image to minimize possible instability artifacts. The standard deviation is calculated in an artifact-free region of interest of the difference image.

To convert from intrinsic SNR to image SNR, we used Eq. [5], with a receiver bandwidth of ±16 kHz and a 256 × 256 acquisition matrix. The pixel volume was 0.16 × 0.16 × 0.15 ml. Naturally, we expect the CPM to have values between 0 and 1.0 at all points. The CPMs of

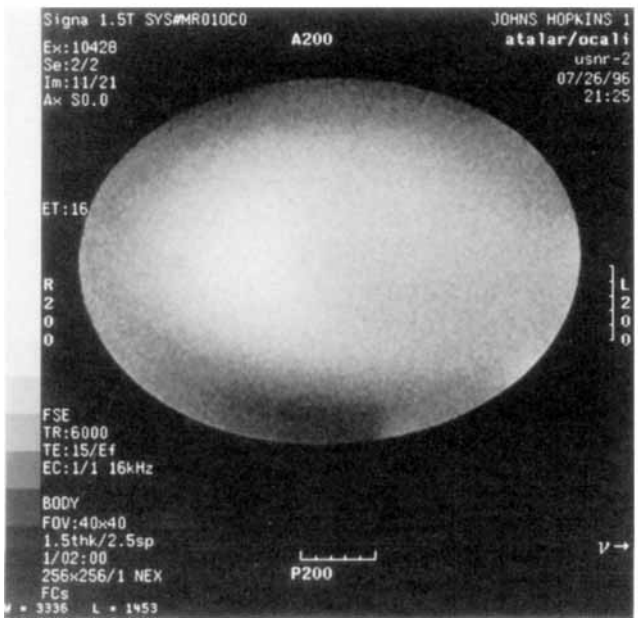

FIG. 6. Torso phantom image using body coil.

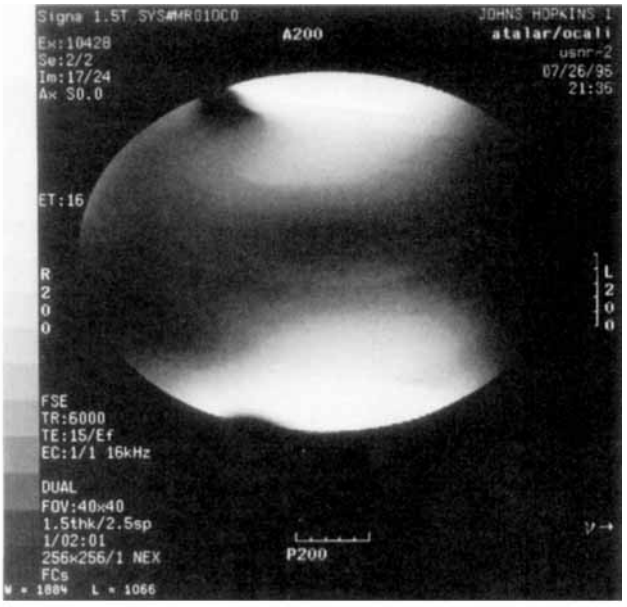

FIG. 7. Torso phantom image using a 5-inch dual coil placed at top and bottom.

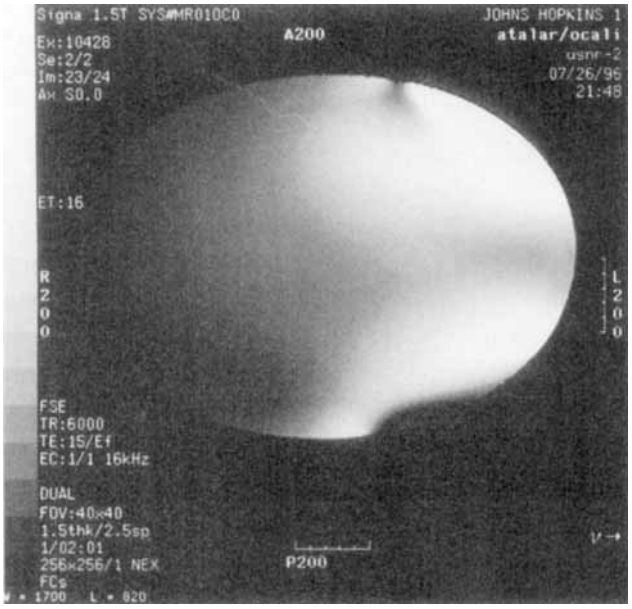

FIG. 8. Torso phantom image using a 5-inch dual coil placed at the side.

the above-mentioned coils are found by using the SNR from the images in Figs. 6–10 and are shown in Figs. 11–15. From these CPMs we can determine the point where the coils get closest to the ultimate performance and how much room there is for further improvement. The cardiac array coil (16) has a point around the heart location at which it achieves almost 80% of the ultimate performance. This performance is very high, considering that we did not incorporate the system losses nor T_1 and T_2 effects. The TR/TE choices of 6 s/14 msec minimize the T_1, T_2 effects, and there is some uncertainty in the MR susceptibility and actual SNR measurements. Yet for the cardiac phased array, we can safely state, based on its CPM, that there is not much room for further improvement. For the dual coil in the top-down arrangement, we observe that there are two distinct peaks in the CPM, which indicate that the coils are either too small or they are separated too much. Note the increase in the CPM when the dual coils are brought closer to the side. Body coil performance is best at the center, but performs less than 36% at all points.

Skin Effect versus Focusing at High Field Strength

We performed simulations for the human torso model described above, with the point of interest at the center of the torso. We calculated the ultimate intrinsic SNR versus the main magnetic field strength for various values of the effective conductivity (see Fig. 16). Effective conductivity of various types of human tissue lies between 0.2 and 1.4 $(\Omega m)^{-1}$ at the frequencies of interest, and in this region our simulations show that ultimate intrinsic SNR increases faster than linearly with the main magnetic field strength below 10 T.

For the case in which effective conductivity equals 0.2 $(\Omega m)^{-1}$, the ultimate intrinsic SNR dependence on B_0 changes from a linear relation, predicted by quasistatic analysis, to an almost cubic relation around $B_0 = 2$ T. This high increase is due to the focusing effect, which is best demonstrated by comparing the sensitivity maps in Fig. 17 at 4.7 T and 10 T with the sensitivity map at 1.5 T (Fig. 4a). Observe that the optimal electromagnetic field is focused at the center, which is our point of interest. Also observe the decrease in focus size as B_0 is increased to 10 T. At high frequencies the wavelength and the focus size become less than the torso dimensions, and the antenna becomes sensitive to noise generated in a small volume of the sample.

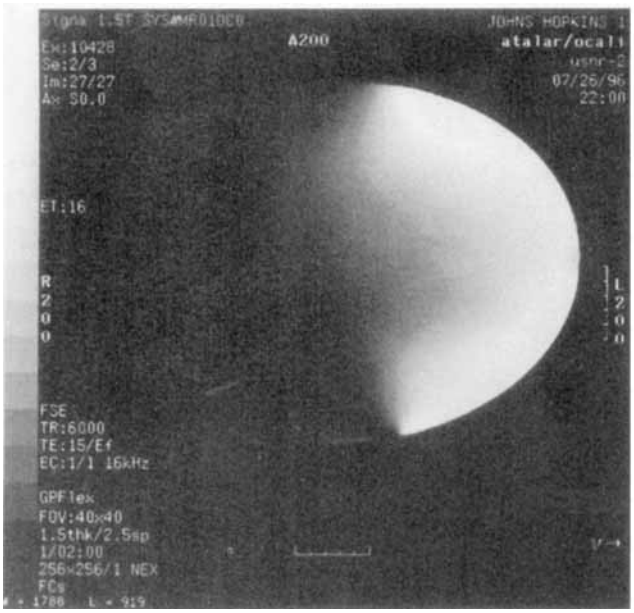

FIG. 9. Torso phantom image using gpflex coil.

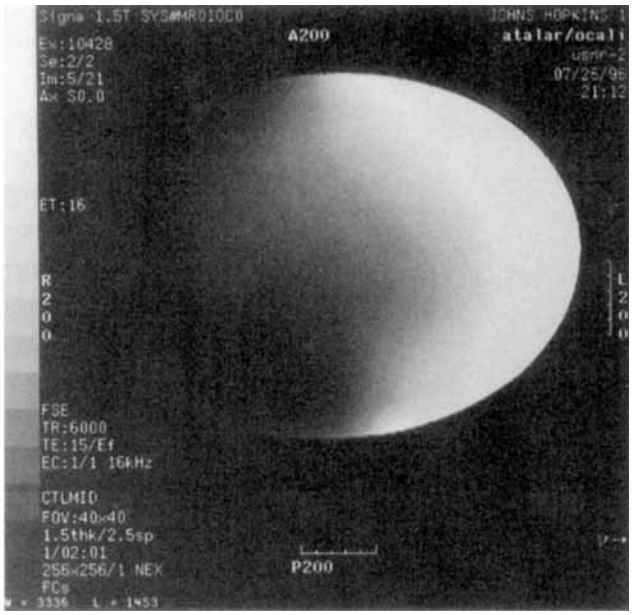

FIG. 10. Torso phantom image using cardiac phased array coil.

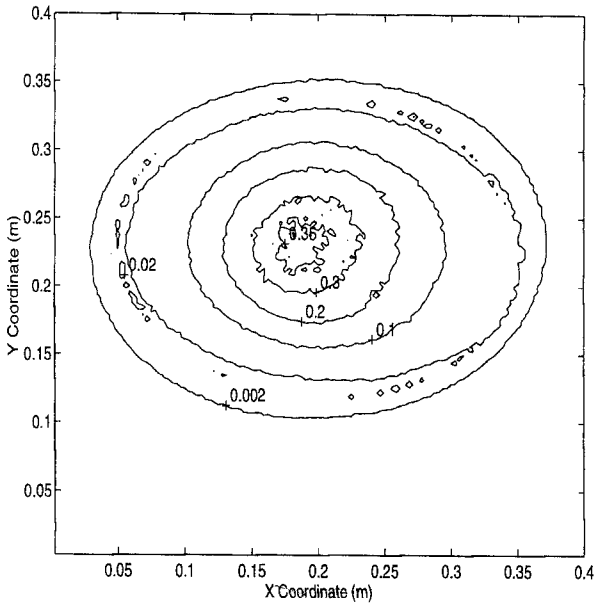

FIG. 11. CPM of body coil.

At low main field strengths (<0.5 T), the value of the ultimate intrinsic SNR is inversely proportional to the square root of the effective conductance, as seen in Fig. 18 (a line with −0.5 slope in a log-log scale). This indicates that the optimal electromagnetic field is almost independent of the conductance, and hence the noise resistance is almost linearly on σ. At high field strengths ultimate intrinsic SNR decreases almost exponentially with increasing conductance because of the skin effect, as seen in Fig. 19 (almost linear dependence in a log-linear scale). In our plots the ultimate intrinsic SNR has a maximum in the range of 0.2–10 T only for $s = 3.2$ and $s = 3.8\ (\Omega m)^{-1}$, well above the human tissue conductivity range.

For our torso model, even when the point of interest is in the center, our results favor the use of high main field strengths. As the point of interest moves closer to the surface, the advantage of a high field strength system will increase. However, to use this advantage, we need coils with focusing capability that are not yet available. As the material conductivity exceeds 2.6 $(\Omega m)^{-1}$ or the body size increases, higher field values will lose their appeal in terms of the ultimate value of intrinsic SNR. Note that this analysis ignores T_1 and T_2 relaxation effects, which are also significant when comparing different field strengths but are beyond the scope of this work.

CONCLUSIONS

A method to calculate the ultimate possible value of the intrinsic SNR for given shapes of homogeneous materials with finite volume is presented. We use *exact* solutions of Maxwell's equations, and the ultimate intrinsic SNR value is determined for totally external sensors.

We compared experimental results from actual coils with the ultimate intrinsic SNR maps. The ultimate intrinsic SNR was used as a reference value in evaluating performances of actual coils and can be used to make design decisions.

The method was then used for comparison of different field strength systems. In terms of ultimate performance, high field strength systems offer more than expected. Our calculations show that the ultimate performance is achieved by focusing the electromagnetic field at the point of interest to compensate for the loss of signal caused by the skin effect. Using this method, we also find the electromagnetic field generated by the optimal MR coil.

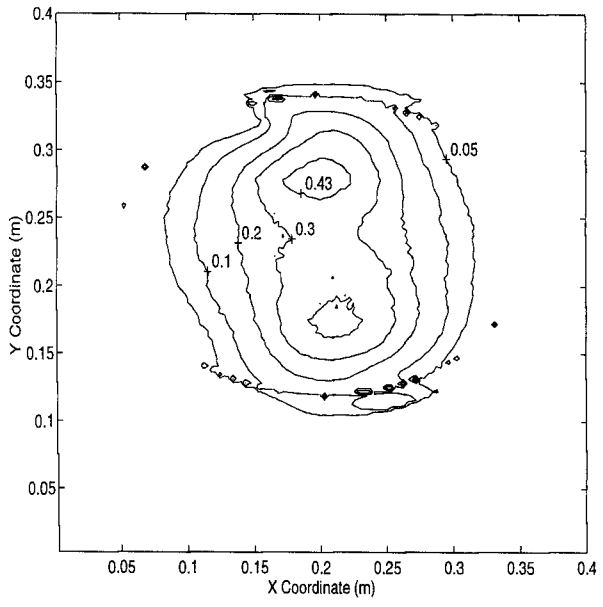

FIG. 12. CPM of 5-inch dual coil placed at top and bottom of the torso phantom.

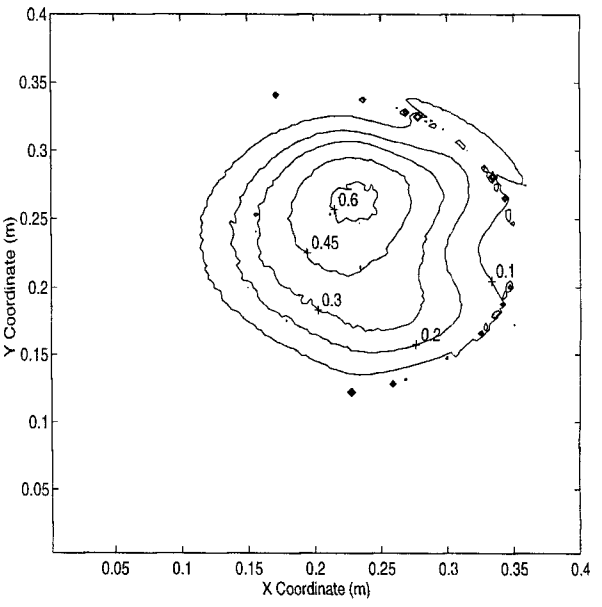

FIG. 13. CPM of 5-inch dual coil placed at the side of the torso phantom.

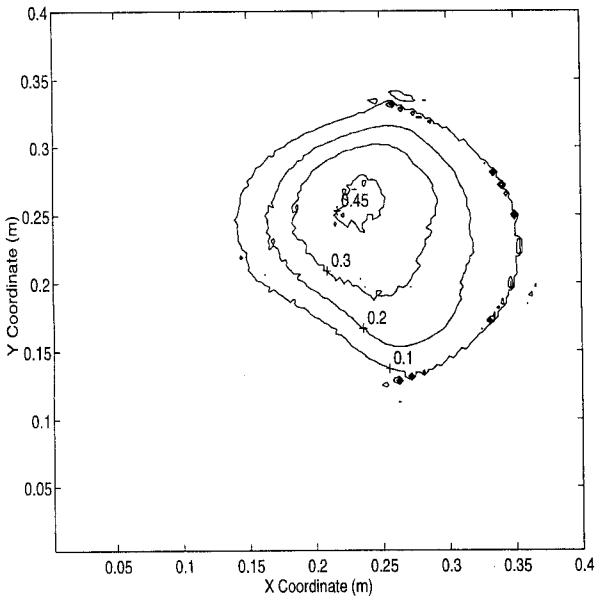

FIG. 14. CPM of gpflex coil.

APPENDIX A

We will prove that the optimal electromagnetic field must satisfy Eq. [10], which we repeat here

$$\int_{\text{body}} \sigma \quad \mathbf{E}^*(\mathbf{r})\mathbf{E}_T(r)\mathrm{d}v = \lambda(H_{T+}(\mathbf{r}_0)) \qquad [A1]$$

$$\lambda = \int_{\text{body}} \sigma \quad |\mathbf{E}(\mathbf{r})|^2\mathrm{d}v \qquad [A2]$$

where $\mathbf{E_T(r)}$, $\mathbf{H_T(r)}$ are arbitrary test fields that also satisfy Maxwell's equations. To that end, we will show that if Eq. [10] is not satisfied for at least one test field, $\mathbf{E_T(r)}$, $\mathbf{H_T(r)}$, then we can improve the original electromagnetic field by adding a small amount of the test function, hence, a contradiction. The test field can be thought of as the electromagnetic field of a potential additional coil; if the optimality condition is not satisfied, we show that it is possible to improve SNR by using the information obtained by the additional coil as an additional element in a linear array.

If the optimality condition is violated for this test field, that is, if

$$\int_{\text{body}} \sigma \quad \mathbf{E}^*(\mathbf{r})\mathbf{E_T(r)}\mathrm{d}v = \lambda'(H_{T+}(\mathbf{r}_0)),\ \lambda' \neq \lambda \qquad [A3]$$

then consider the new electromagnetic field, $\mathbf{E}_\epsilon(\mathbf{r})$, $\mathbf{H}_\epsilon(\mathbf{r})$, which is an ϵ parametric linear combination of the original and the test field

$$\mathbf{E}_\epsilon(\mathbf{r}) = \frac{\mathbf{E(r)} - \epsilon[(\lambda' - \lambda)H_{T+}(\mathbf{r}_0)]^*\mathbf{E_T(r)}}{1 - \epsilon[(\lambda' - \lambda)H_{T+}(\mathbf{r}_0)]^*H_{T+}(r_0)} \qquad [A4]$$

$$\mathbf{H}_\epsilon(\mathbf{r}) = \frac{\mathbf{H(r)} - \epsilon[(\lambda' - \lambda)H_{T+}(\mathbf{r}_0)]^*\mathbf{H_T(r)}}{1 - \epsilon[(\lambda' - \lambda)H_{T+}(\mathbf{r}_0)]^*H_{T+}(r_0)} \qquad [A5]$$

Because $\mathbf{E}_\epsilon(\mathbf{r})$, $\mathbf{H}_\epsilon(\mathbf{r})$ is a linear combination of the original and the test electromagnetic fields, and both satisfy Maxwell's equations which are linear, the new electromagnetic field also satisfies Maxwell's equations. Moreover, the new magnetic field at the point of interest is

$$H_{\epsilon+}(\mathbf{r}_0) = \frac{H_+(\mathbf{r}_0) - \epsilon[(\lambda' - \lambda)H_{T+}(\mathbf{r}_0)]^*H_{T+}(\mathbf{r}_0)}{1 - \epsilon[(\lambda' - \lambda)H_{T+}(\mathbf{r}_0)]^*H_{T+}(\mathbf{r}_0)} \qquad [A6]$$

$$= 1 \qquad [A7]$$

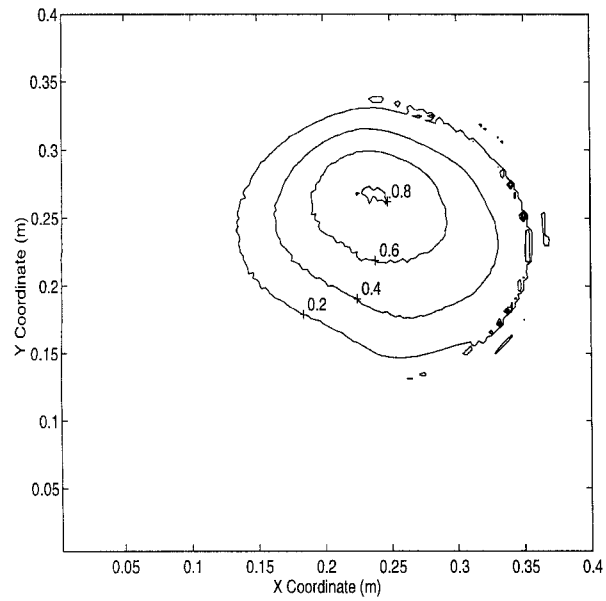

FIG. 15. CPM of cardiac phased array.

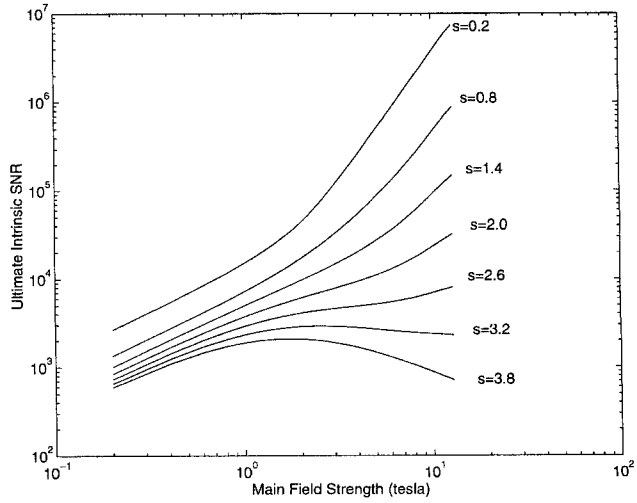

FIG. 16. Ultimate intrinsic SNR versus main field strength at the center of the human torso model for different values of effective conductance *s*.

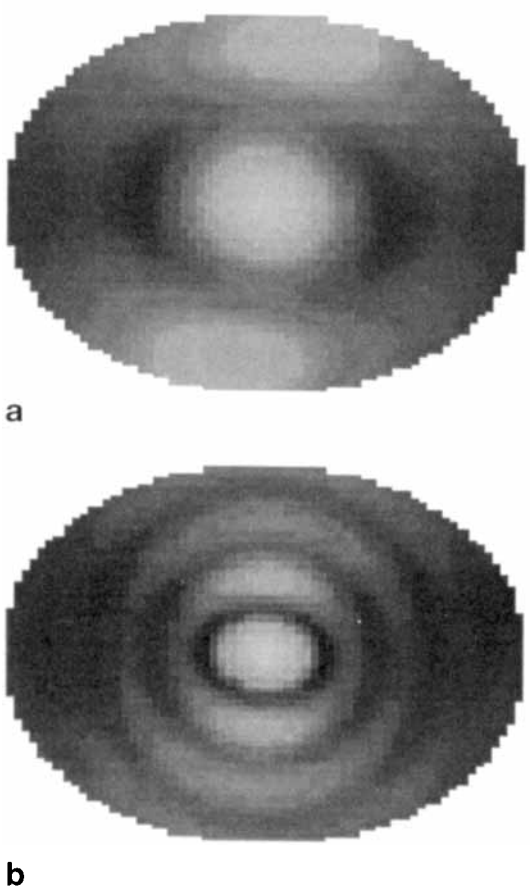

FIG. 17. The right-hand polarized component of the electromagnetic field (sensitivity) optimized at the center of the torso for main field strength (a) 4.7 T, (b) 10 T. Note the decrease in the focus size as the field increases.

which is true for all values of ϵ, because the original electromagnetic field has a unity sensitivity at the point of interest.

Calculating the deposited power for the new combined field we find

$$\int_{\text{body}} \sigma \quad \mathbf{E}_{\epsilon}^{*}(\mathbf{r})\mathbf{E}_{\epsilon}(\mathbf{r})\mathrm{d}v$$

$$= \frac{\int_{\text{body}} \sigma \quad [\mathbf{E}^{*}(\mathbf{r})\mathbf{E}(\mathbf{r}) - \epsilon[(\lambda' - \lambda)H_{T+}(\mathbf{r}_0)]\mathbf{E}^{*}(\mathbf{r})\mathbf{E}_T(r)]\mathrm{d}v}{|1 - \epsilon[(\lambda' - \lambda)H_{T+}(\mathbf{r}_0)]^{*}H_{T+}(\mathbf{r}_0)|^2}$$

$$- \frac{\int_{\text{body}} \sigma \quad \epsilon[(\lambda' - \lambda)H_{T+}(\mathbf{r}_0)]\mathbf{E}(\mathbf{r})\mathbf{E}_T^{*}(r)\mathrm{d}v}{|1 - \epsilon[(\lambda' - \lambda)H_{T+}(\mathbf{r}_0)]^{*}H_{T+}(\mathbf{r}_0)|^2} \qquad [A8]$$

$$+ \frac{\int_{\text{body}} \sigma \quad |\epsilon[(\lambda' - \lambda)H_{T+}(\mathbf{r}_0)]^{*}\mathbf{E}_{\mathbf{T}}(\mathbf{r})|^2\mathrm{d}v}{|1 - \epsilon[(\lambda' - \lambda)H_{T+}(\mathbf{r}_0)]^{*}H_{T+}(\mathbf{r}_0)|^2}$$

By performing a Taylor expansion of Eq. [A8] in powers of ϵ, and dividing both sides by σ one obtains

$$\int_{\text{body}} \sigma \quad \mathbf{E}_{\epsilon}^{*}(\mathbf{r})\mathbf{E}_{\epsilon}(\mathbf{r})\mathrm{d}v \qquad [A9]$$

$$= \lambda - 2\epsilon|(\lambda' - \lambda)H_{T+}(\mathbf{r}_0)|^2 + \mathbb{O}(\epsilon^2)$$

where $\mathbb{O}(\epsilon^2)$ takes the terms with second or higher powers of ϵ into consideration. Hence, the deposited power for the new combined electromagnetic field can be made less than that of λ by choosing $\epsilon > 0$ sufficiently small, and the new field is better than the original field in terms of SNR.

APPENDIX B

The entries of the R matrix (noise correlation matrix) can be computed as follows.

$$R_{ij} = \sigma \int_{\text{body}} \mathbf{E}_i(\mathbf{r}_p)^{*}\mathbf{E}_j(\mathbf{r}_p)\mathrm{d}v_p \qquad [B1]$$

and the row vector, $\mathbf{b} \in \mathbb{C}^{1\times n}$, (sensitivity matrix) as follows:

$$b_i = H_{i+}(r_0) \qquad [B2]$$

where $\mathbf{H}_{i+}$ denotes the right-hand circularly polarized component of the H field of the i^{th} mode in the x, y plane. With our definitions of the modes it becomes

$$H_{i+} = \frac{H_{i0_x} + jH_{i0_y}}{\sqrt{2}} \qquad [B3]$$

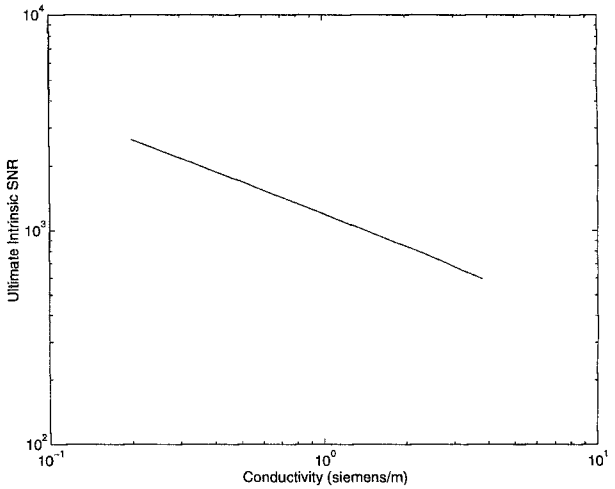

FIG. 18. Ultimate intrinsic SNR versus effective conductance at low main field strength (0.2 T). Observe that the log-log plot has about −1/2 slope, which is in accordance with the quasistatic assumptions.

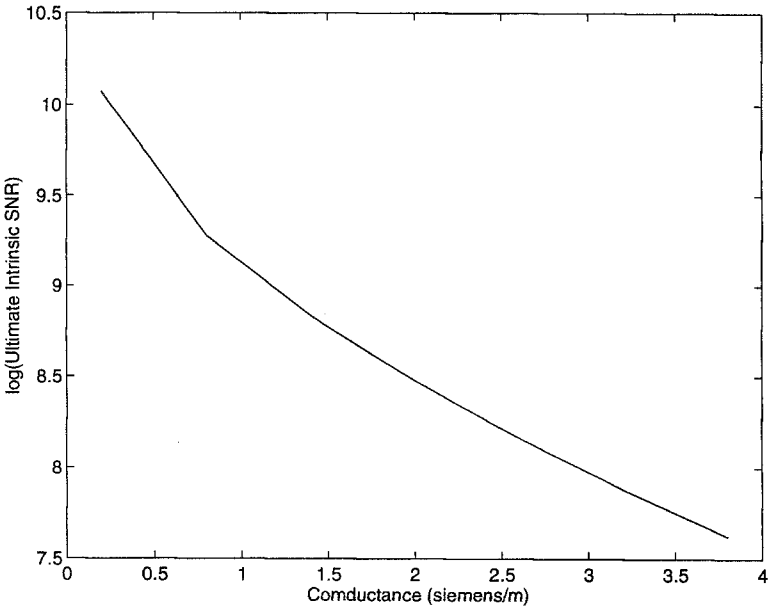

FIG. 19. Ultimate intrinsic SNR versus effective conductance at high main field strength (10 T). Note the exponential dependence of the ultimate intrinsic SNR on the conductance indicating the skin effect.

For a cube centered at the origin with edges of $2 * l$ length, the computation of R_{ij} is as follows, using Eq. [24]

$$R_{ij} = \sigma \int_{\text{body}} \mathbf{E}_i(\mathbf{r}_p)^* \mathbf{E}_j(\mathbf{r}_p) dv_p \qquad [B4]$$

$$= \sigma \mathbf{E}^*_{\mathbf{i0}} \mathbf{E}_{\mathbf{j0}} \int_{\text{body}} e^{-j(\mathbf{k}_j - \mathbf{k}_i^*)\cdot \mathbf{r}} dv \qquad [B5]$$

$$= \sigma \mathbf{E}^*_{\mathbf{i0}} \mathbf{E}_{\mathbf{j0}}\, D_l(k_{jx} - k^*_{ix})\, D_l(k_{jy} - k^*_{iy})\, D_l(k_{jz} - k^*_{iz}) \qquad [B6]$$

where $k_{ix}, k_{iy}, k_{iz} \in \mathbb{C}$ denote the x, y, z component of the i^{th} wave vector and the function $D_l(\cdot)$ is given as

$$D_l(\alpha) = \frac{2 \sin(\alpha l)}{\alpha} \qquad [B7]$$

and if the parameter α equals zero, D_l takes the value $2l$. Observe that k_{ix}, k_{iy}, k_{iz} may take complex values. In that case we adhere to the definition of sinus function

$$\sin(x) = \frac{e^{jx} - e^{-jx}}{2j} \qquad [B8]$$

This computation is easily extended to a filled rectangular box by simply scaling the axes. Observe that computing R is equivalent to evaluating the 3D Laplace transform of a function that has the value, $\sigma \mathbf{E}^*_{\mathbf{i0}} \mathbf{E}_{\mathbf{j0}}$, inside the body and 0 outside the body.

In the case of a filled cylinder with a circular profile, the computation of b is exactly the same. Assuming a length of $2*l$ along the z direction, with radius, r_c,

$$R_{ij} = \sigma \mathbf{E}^*_{\mathbf{i0}} \cdot \mathbf{E}_{\mathbf{j0}} \int_{\text{body}} e^{-j(\mathbf{k}_j - \mathbf{k}_i^*)\cdot \mathbf{r}} dv \qquad [B9]$$

$$= \sigma \mathbf{E}^*_{\mathbf{i0}} \cdot \mathbf{E}_{\mathbf{j0}} \int_{-l}^{l} e^{-j(k_{jz} - k^*_{iz})z} dz \cdot \int_0^{r_c} r dr \int_0^{2\pi} e^{-jr[(k_{ix} - k^*_{jx})\cos(\theta) + (k_{iy} - k^*_{jy})\sin(\theta)]} \qquad [B10]$$

$$= \sigma \mathbf{E}^*_{\mathbf{i0}} \cdot \mathbf{E}_{\mathbf{j0}}\, D_l(k_{jz} - k^*_{iz}) \frac{2}{k} \sqrt{\frac{\pi}{2}}\, r_c J_1(k r_c) \qquad [B11]$$

where $J_1(\cdot)$ denotes the first-order ordinary Bessel function [17], and $k = [(k_{jx} - k^*_{ix})^2 + (k_{jy} - k^*_{iy})^2]^{1/2}$.

In the case where the profile is elliptic, defined by the equation

$$\frac{x^2}{c^2} + y^2 = r_c^2 \qquad [B12]$$

the computation of the **b** matrix is the same, but for computation of the **R** matrix we must make the scaling coordinate transformation

$$x' = \frac{x}{c} \qquad [B13]$$

which gives us the result

$$R_{ij} = \sigma \mathbf{E}^*_{\mathbf{i0}} \cdot \mathbf{E}_{\mathbf{j0}}\, D_l(k_{jz} - k^*_{iz}) \frac{2}{k} \sqrt{\frac{\pi}{2}}\, r_c J_1(k' r_c) \qquad [B14]$$

where $k' = [c^2(k_{jx} - k^*_{ix})^2 + (k_{jy} - k^*_{iy})^2]^{1/2}$.

Because the medium is lossy, the wave vector is, in general, complex valued. Thus, we must evaluate the Bessel function for complex arguments. We use a series approximation for the Bessel function (17).

ACKNOWLEDGMENTS

Special thanks to Paul E. Bottomley for providing the experimental cardiac phased array and Mary McAllister for her help in manuscript preparation. We also thank Ayhan Altintas and Elliot R. McVeigh for their valuable comments.

REFERENCES

1. W. A. Edelstein, G. H. Glover, C. J. Hardy, R. W. Redington, The intrinsic signal-to-noise ratio in NMR imaging. *Magn. Reson. Med.* **3,** 604–618 (1986).
2. J. Wang, A. Reykowski, J. Dickas, Calculation of the signal-to-noise ratio for simple surface coils and arrays of coils. *IEEE Trans. Biomed. Eng.* **42,** 908–917 (1995).
3. P. A. Bottomley, E. R. Andrew, RF magnetic field penetration, phase shift and power dissipation in biological tissue: implication on NMR imaging. *Phys. Med. Biol.* **23,** 630–643 (1978).
4. D. I. Hoult, P. C. Lauterbur, The sensitivity of the zeugmatographic experiment involving human samples. *JMR* **34,** 425–433 (1979).
5. H. Vesselle, R. E. Collin, The signal-to-noise ratio of nuclear magnetic resonance surface coils and application to a lossy dielectric cylinder model: Part I. Theory. *IEEE Trans. Biomed. Eng.* **42,** 497–506 (1995).
6. P. B. Roemer, W. A. Edelstein, Ultimate sensitivity limits of surface coils. *Magn. Reson. Med.* **1,** 410 (1986).
7. W. Schnell, M. Vester, W. Rentz, H. Ermert, Ultimate SNR of superposition of radial and azimuthal dipoles surrounding a lossy cylinder. *In* "Proc., ISMRM 4th Scientific Meeting, New York, 1996." p. 1445.
8. R. M. Henkelman, Measurement of signal intensities in the presence of noise in MR images. *Med. Phys.* **12,** 232–233 (1985).
9. S. Ramo, J. R. Whinnery, T. V. Duzer, "Fields and Waves in Communication Electronics," 2nd ed., John Wiley and Sons, New York, 1984.
10. E. Yamashita, editor, "Analysis Methods for Electromagnetic Wave Problems," vol. 1, Artech House, Boston. London, 1990.
11. R. Rudduck, C.-L. Chen, New plane wave spectrum formulations for the near fields of circular and strip apertures. *IEEE Trans. Antennas Propagation,* **AP-24,** 238–239 (1976).
12. P. C. Clemmow, "The Plane Wave Representation of Electromagnetic Fields," Pergamon Press, New York, 1966.
13. P. B. Roemer, W. A. Edelstein, C. E. Hayes, S. P. Souza, O. M. Muller, The NMR phased array. *Magn. Reson. Med.* **16,** 192–225 (1990).
14. A. Abragam, "Principles of Nuclear Magnetism, The International Series of Monographs on Physics." Oxford University Press, Oxford, England, 1986.
15. A. Casaleggio, C. Martini, M. Morando, S. Ridella, G. S. Mela, L. Spiga, E. Intra, Electrical behavior of human sera between 50–1000 MHz, *in* "Interactions between Electromagnetic Fields and Cells," pp. 100–115. Plenum Press, New York, 1984.
16. P. A. Bottomley, C. H. L. Olivieri, What is the optimum phased-array coil design for cardiac magnetic resonance? *in* "Proc., ISMRM 4th Scientific Meeting, New York, 1996," p. 248.
17. I. S. Gradhsteyn, I. M. Ryhzik, "Table of Integrals, Series, and Products." Academic Press, Inc., Orlando, 1980.